16

Mechanical Durability of Inorganic Films on Flexible Substrates

Yves Leterrier

Laboratoire de Technologie des Composites et Polymères (LTC), Ecole Polytechnique Fédérale de Lausanne (EPFL), Lausanne, Switzerland

16.1 Introduction

Flexible electronics such as flexible displays are multilayer structures based on substrates foils engineered with a diversity of thin-film architectures [1, 2]. Flexibility goes together with thinness: present devices (liquid crystals, electrophoretic displays, organic light-emitting diodes) are intrinsically thin, and corresponding displays are thus flexible when using thin substrates. Nevertheless, the extent to which, and the number of times flexible display structures can be safely bent are essential, but highly challenging design features [3]. An outstanding issue related to mechanical integrity is the lack of understanding of the key factors that control damage processes such as film cracking and interfacial delamination. The reason is the considerable property contrast between substrate and coating materials and associated complex distortion and damage problems. Polymer materials used as substrates are much less rigid and much more sensitive to changes of temperature and relative humidity than inorganic materials such as oxides used as e.g. passivation, diffusion barrier, and transparent conducting layers. In contrast polymers are usually much more robust than inorganic materials. In addition, the small dimensions of the film material with thickness often in the sub-micron range add a great deal of complications for experimental analyses of mechanical properties. Mechanical models and test methods relevant for thin films on polymers have emerged in the last 20 years [4]. Progress in the field of thin-film mechanics is very active, stimulated by the development of novel designs, improved fabrication processes and new materials with increased mechanical stability. In spite of such knowledge, design and process engineers working on the implementation of flexible electronics may still lack confidence due to a general lack of understanding, or lack of input data for reliable modeling tools.

The aim of this chapter is to introduce basic mechanical concepts and provide key ingredients for rational design of flexible display structures, with focus on critical strain for damage and associated critical radius of curvature. Section 16.2 introduces important materials for flexible displays and highlights their property contrast. Section 16.3 is devoted to the analysis of stresses and strains and related critical radius of multilayer structures, with attention paid to process-induced internal strains. Section 16.4 details the main test methods and the analysis of failure mechanisms under tensile and compressive loading, and are illustrated with case studies from the literature. Section 16.5 is devoted to durability influences, including the effect of temperature, fatigue, and corrosion. Section 16.6 is a short review of the development of robust, "unbreakable" films and layer materials relevant to flexible displays. Section 16.7 closes this chapter.

Flexible Flat Panel Displays, Second Edition. Edited by Darran R. Cairns, Dirk J. Broer, and Gregory P. Crawford.

16.2 Flexible Display Materials

16.2.1 Property Contrast between Coating and Substrate Materials

Table 16.1 compiles representative flexible display substrates and functional layers, their process methods, and representative thickness. Substrates are generally polymer foils, with thermomechanical properties in striking contrast with those of functional display layers (essentially brittle oxides and nitrides) as shown in Figure 16.1. Steel and glass foils are interesting alternatives to polymers, being thermally stable and perfect diffusion barriers. However, steel is not transparent and both steel and glass yields/fractures at very low strains. As will be discussed later, a key property regarding the mechanical stability of flexible display structures is the critical strain, at which mechanical damage occurs, be it in the form of cohesive failure of brittle films, or adhesive failure at a film/substrate interface.

16.2.2 Determination of Mechanical Properties of Inorganic Coatings

The determination of critical conditions (curvature, stretch, temperature) for mechanical failure of a display requires knowledge of several features and properties of individual layer materials, namely their Young's modulus, Poisson's ratio, coefficients of thermal and hygroscopic expan-

Table 16.1 Substrates foils and coating layers used in flexible displays

Function	Material	Process method	Typical thickness
Substrate	Elastomers (PDMS)	Solution cast	1 mm
[5]	Polymers (PI, PET, PEN, PES ...)	Solution cast, extrusion – stretched	10–200 μm
	Paper	Water slurry + lamination	100 μm
	Steel	Cold rolling	100 μm
	Glass	Float and fusion	30–600 μm
Passivation/ diffusion barrier	SiN_x	Chemical vapor deposition	50–1000 nm
	SiO_x	Chemical vapor deposition	10–500 nm
[6, 7]	Al_2O_3, ZrO_2	Atomic layer deposition	10–300 nm
	Parylene C	Vapor deposition	0.2–100 μm
	Polymer nanocomposite	Solution cast	1–10 μm
Transparent	Sn-doped In oxide, ITO	Vapor deposition	100–200 nm
electrode [8, 9]	Al, Ga or In-doped zinc oxide (AZO, GZO, IZO)	Vapor deposition/Solution cast + annealed	0.1–5 μm
	Graphene and carbon nanotube polymer composites	Compounding	1–10 μm
	Conducting polymers (e.g. PEDOT-PSS[1])	Solution cast	10–100 nm
TFT [10, 11]	Si (amorphous, microcrystalline, polycrystalline)	Chemical vapor deposition	100 nm

(1) poly(3,4-ethylenedioxythiophene):poly(styrene sulfonate)

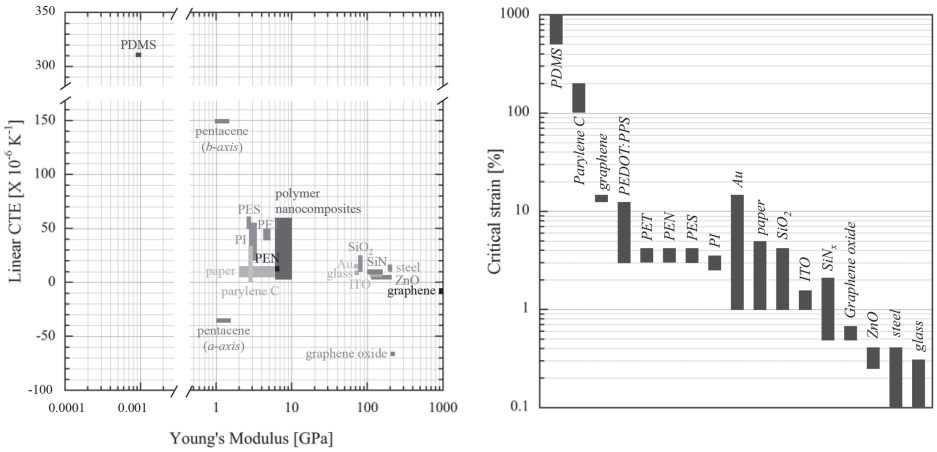

Figure 16.1 Young's modulus (log-scale) versus coefficient of thermal expansion (left) and critical strain for tensile failure (fracture strain or yield strain, right) of relevant flexible display materials. Data ranges reflect the diversity of process-induced microstructures in these various materials.

sion (CTE and CHE), thickness, and critical strain. Methods to determine the latter in the case of tensile and compressive loading situations will be detailed in Section 16.4.

Nanoindentation techniques are well established to measure the elastic modulus of films on substrates [12] including flexible polymer substrates [13]. Nanoindentation is also used to determine the fracture [14] and adhesion [15] properties of coatings on flexible substrates. In a nanoindentation experiment a specimen is indented with a sharp tip while measuring the indentation load and displacement during both loading and unloading [16–18]. Doerner and Nix have proposed the following empirical dependence of the effective modulus of the sample, E, on the normalized indentation depth h_{ind}/h_f, using an adjustable parameter ξ [19]:

$$\frac{1}{E} = \frac{w}{E_f} + \frac{1-w}{E_s} \quad where \quad w = 1 - \exp\left\{-\xi \frac{h_f}{h_s}\right\} \tag{16.1}$$

In case of high elastic contrast (stiff film on soft substrate) the indentation depth is recommended to be much less than 10% of the film thickness, possible 1% to minimize substrate influence [12]. The accuracy of the method is compromised by the presence of "third-body interactions" such as indenter-film friction and the occurrence of so-called "piling up." These issues and data-processing models were reviewed in detail by [20] and [21]. Figure 16.2 compares experimental data for films deposited on stiff substrates with Equation 16.1. It is evident that as indentation depth increases the effective modulus progressively converges toward that of the substrate. The application of Equation 16.1 leads to accurate determination of the Young's modulus of films with sub-micron thickness.

Alternative methods to determine the Young's modulus of thin films include tensile tests using thin substrates and the classic laminate plate theory [22], buckling analyses [23, 24], acoustic and heterodyne atomic force microscopy [25], surface acoustic wave methods [26, 27], and scanning local acceleration microscopy [28].

Conventional mechanical and dilatometry test methods can be used to measure the Poisson's ratio, CTE, and CHE of film samples with thicknesses above a few microns (the Poisson's ratio

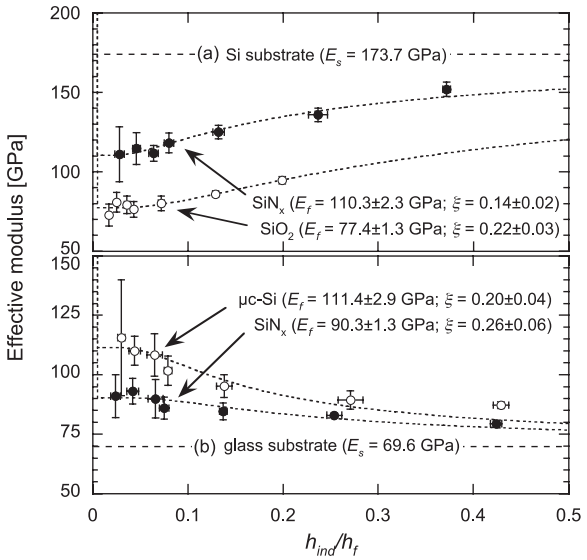

Figure 16.2 Effective modulus versus normalized indentation depth for selected films on Si (a) and glass (b) substrates. Symbols are experimental data and dashed lines represent Equation (16.1). Best-fit values for film modulus E_f and indentation parameter ξ are indicated.

has a small influence on calculated properties and approximate values are usually sufficient). However, these measurements are highly challenging for films with thickness in the sub-micron range. Approaches to determine the CTE and CHE are described in Section 16.3.1.

16.3 Stress and Strain Analyses

The strain in a flexible display structure being curved is the combination of internal strains and bending strains as depicted in Figure 16.3 and detailed in the following. Excessive strain levels may relax through cracking and delamination. Internal strains are primarily controlled by the fabrication process, and by changes of e.g. temperature during service, whereas bending strains result from the applied curvature.

16.3.1 Intrinsic, Thermal, and Hygroscopic Stresses and Strains

Internal stresses (often referred to as residual stresses) and strains in vapor-deposited and solution-processed films and coatings generally include intrinsic, thermal, and hygroscopic contributions whose process dynamics are sketched in Figure 16.4 [29–33]. Intrinsic stresses are associated with process-induced disorder (tensile or compressive in inorganic films) and a number of shrinkage mechanisms (generally tensile in organic films). Thermal stresses develop upon cool-down from process temperature or upon temperature variations during service because material constituents have mismatched thermal expansion coefficients. Thermal stresses are generally compressive in inorganic films and maybe tensile or compressive in organic films, when using polymers as substrates. Hygroscopic stresses also develop upon exposure to ambient humidity, due to a mismatch in hygroscopic expansion between material constituents. Hygroscopic stresses

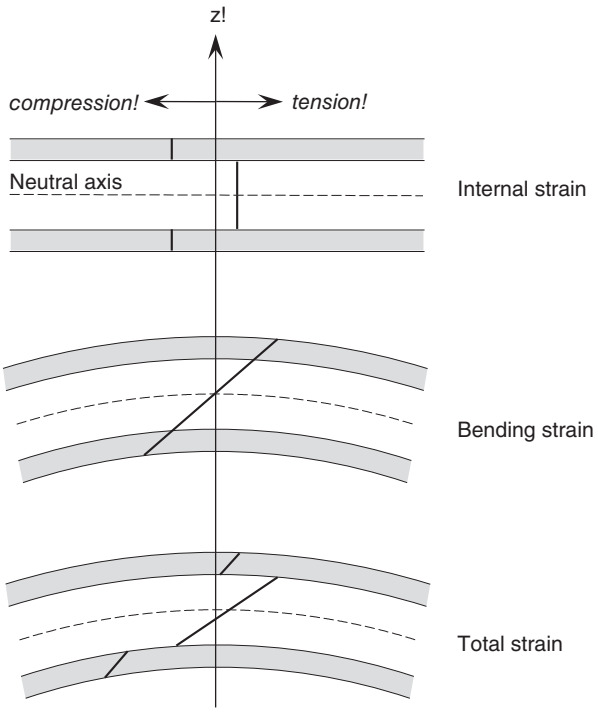

Figure 16.3 Sketches of internal, bending, and total strain profiles in a symmetric three-layer structure (substrate coated on both sides with identical coating). The total strain is the sum of the internal and bending strains.

are generally tensile in inorganic films and can be tensile or compressive in organic films. Additional stresses may develop during post-deposition processes due to further dimensional changes of the polymer substrate, such as upon unloading from roll-to-roll manufacturing [34].

The internal strain $\varepsilon_i = \varepsilon_i^{in} + \varepsilon_i^{th} + \varepsilon_i^{hy}$ includes intrinsic, thermal, and hygroscopic contributions, with:

$$\varepsilon_i^{th} = \Delta\alpha\,\Delta T = (\alpha_s - \alpha_f)(T - T_0) \tag{16.2a}$$

$$\varepsilon_i^{hy} = \Delta\beta\,\Delta RH = (\beta_s - \beta_f)(RH - RH_0) \tag{16.2b}$$

where α_s and α_f are the CTE of substrate and film, T is the actual temperature, and T_0 is the process temperature (which would correspond to a stress-free temperature in the case where the intrinsic strains would be zero), β_s and β_f are the CHE of substrate and film, RH is the actual relative humidity, and RH_0 the relative humidity of the process (zero in the case of vacuum deposition).

The two main methods to measure the internal strain in films on substrates (from which the internal stress can be calculated providing that the elastic constants of the film are known) are x-ray diffraction and bilayer curvature measurements. X-ray diffraction is limited to crystalline materials and provides accurate determination of internal strain from the change of lattice spacing, and associated change of scattering angle. The $\sin^2\psi$ method, where ψ is the declination

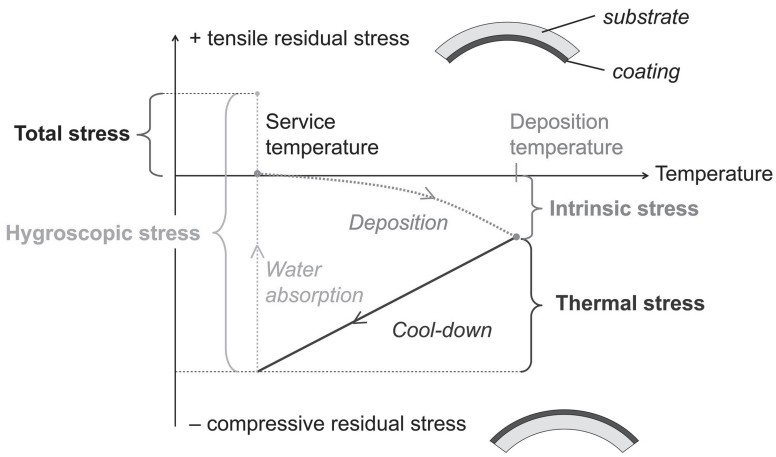

Figure 16.4 Residual stress dynamics during vacuum deposition of films on polymer substrates. The intrinsic stress (compressive in the figure) can be either tensile or compressive. The tensile stress is usually compressive. The hygroscopic stress is usually tensile. The total stress (tensile in the figure) can be either tensile or compressive. Reproduced with permission from [35].

angle between the normal to the film surface and the scattering vector, moreover enables measurement of the elasticity coefficients of the film for isotropic materials [36, 37].

The bilayer curvature measurements rely on the analysis of the equilibrium curvature of a film/substrate system resulting from the presence of internal strains. The film/substrate system can adopt the shape of a spherical cap (isotropic strain and stiff substrate), a saddle shape, or a roll (compliant substrate) depending on the geometry of the system, the thickness and elastic properties of the constituents, and on the degree of in-plane anisotropy of the internal strain. For samples in the form of narrow strips (i.e. with main curvature along the length of the strip) the in-plane film strain can be calculated using the classic Stoney equation (actually its in-plane biaxial stress version) [38]:

$$\varepsilon_i = -\frac{\left(1-\nu_f\right)E_s h_s^2}{6\left(1-\nu_s\right)E_f h_f}\left(\frac{1}{R_2}-\frac{1}{R_1}\right) \tag{16.3}$$

where h_i, ν_i, and E_i represent the thickness, Poisson's ratio, and Young's modulus of layer i (subscripts f and s for film and substrate, respectively), and R_2 and R_1 are the radii of curvature of the coated substrate and of the plain substrate, respectively. The "–"sign is a convention (compressive strains are negative and tensile strains are positive). In case of a large elastic contrast between film and substrate the following correction to Stoney's equation should be used [39]:

$$\varepsilon_i = -\frac{\left(1-\nu_f\right)\left(1+\eta\left(4\chi-1\right)\right)h_s}{6\left(1-\nu_s\right)\eta\chi}\left(\frac{1}{R_2}-\frac{1}{R_1}\right) \tag{16.4}$$

where $\eta = h_f/h_s$ and $\chi = E_f/E_s$. This equation is valid for small deflections (compared with the sample dimensions). Refined models are detailed in [32] and the case of large deflections is treated in [40].

Figure 16.5 regroups internal stress data for transparent conductive oxides (TCOs) [41] and diffusion barrier [35] films, which highlights the influence of process conditions (Figure 16.5a

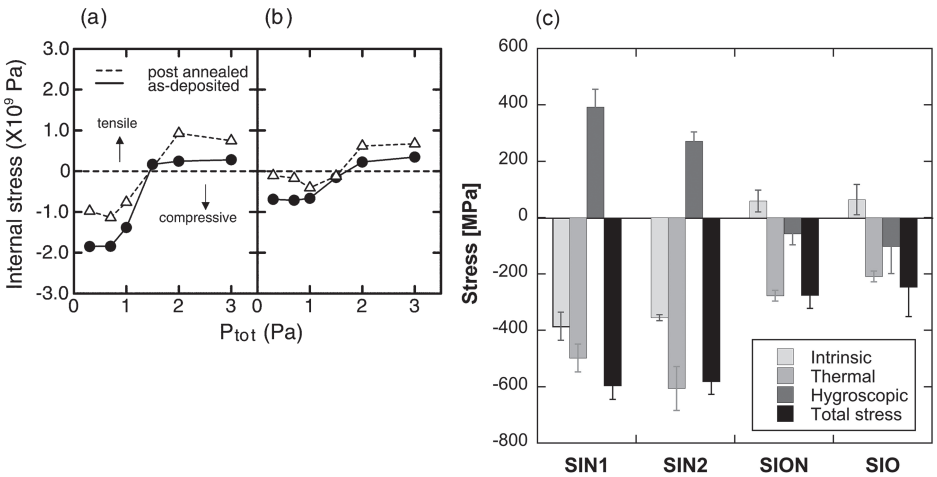

Figure 16.5 Internal stress in (a) ITO and (b) IZO films (thickness: 180–240 nm) deposited on glass substrates by r.f. magnetron sputtering without substrate heating under various total gas pressures (P_{tot}) before and after post-annealing in air at 250°C for 1 hour (reproduced with permission from [41]) and internal stress components (c) in 400-nm thick silicon nitride (SIN 1, SIN2), silicon oxinitride (SION) and silicon oxide (SIO) coatings on a 125 μm PI substrate at 22°C and 50% RH (positive stresses are tensile and negative stresses are compressive; reproduced with permission from [35]).

and b) and composition (Figure 16.5c) on the magnitude and nature (tensile or compressive) of the stress. These data are particularly useful to reduce internal stresses and even produce stress-free layers. The individual components of the in-plane film strain such as shown in Figure 16.5c are identified using the protocol detailed in [33]. The intrinsic strain is obtained in a first step, from the analysis of the film/substrate curvature measured under the conditions prevalent at the end of the process cycle (e.g. vacuum, temperature). The temperature-dependent thermal strain and humidity-dependent hygroscopic strain are obtained from the change of curvature of the film/substrate subjected to iso-hygric temperature jumps and isothermal relative humidity jumps, respectively. This approach combined with modeling tools enabled derivations of the CTE and CHE of thin-film materials, using known CTE and CHE of substrate materials (see also [42]).

16.3.2 Strain Analysis of Multilayer Films under Bending

The strain (stress) in multilayer film structures under bending is a linear superposition of the internal process-induced strain (stress) previously detailed and externally applied bending strain (stress), as sketched in Figure 16.3:

$$\varepsilon = \varepsilon_b + \varepsilon_i \tag{16.5}$$

The bending strain ε_b is proportional to the distance z from the neutral axis with maximum tensile strain on the top (convex) surface and maximum compressive strain on the bottom (concave) surface:

$$\varepsilon_b = a_0 + a_1 z \tag{16.6}$$

where a_0 and a_1 are constants. The neutral axis is the line within the multilayer structure where the strain does not change upon pure bending. The position z_{NA} of the neutral axis in a multilayer (taking the free surface of the first layer as the origin $z = 0$) is given by:

$$z_{NA} = \frac{\sum_{i=1}^{N} \bar{E}_i h_i \bar{z}_i}{\sum_{i=1}^{N} \bar{E}_i h_i} \tag{16.7}$$

where $\bar{E}_i = E_i / (1 - \nu_i^2)$ is the plane strain modulus of layer i (E_i and ν_i are its Young's modulus and Poisson's ratio, respectively), $\bar{z}_i$is the position of the mid-plane of layer i, h_i is the thickness of layer i, and N is the number of layers.

16.3.3 Critical Radius of Curvature

The critical radius of curvature, R_{crit}, at which device failure occurs is among the key design parameters for flexible electronics. For the elastic case (dissipative processes such as substrate yielding are not considered) and in the case of pure bending R_{crit} is inversely proportional to the critical strain ε_{crit} (related to either cohesive failure of a layer, or interfacial failure) [43]:

$$R_{crit} = \left(\frac{h_f + h_s}{2\varepsilon_{crit}} \right) \left(\frac{1 + 2\eta + \chi\eta^2}{(1+\eta)(1+\chi\eta)} \right) \tag{16.8}$$

which simplifies in the case $h_f \ll h_s$ ($\eta \ll 1$) and $E_f < \sim 10\, E_s$ ($\chi < \sim 10$):

$$R_{crit} \approx \frac{h_s}{2\varepsilon_{crit}} \tag{16.9}$$

Figure 16.6 plots the normalized strain in the film versus film/substrate thickness ratio, calculated using Equation 16.8. Two kinds of substrates are compared: steel (Young's modulus ratio

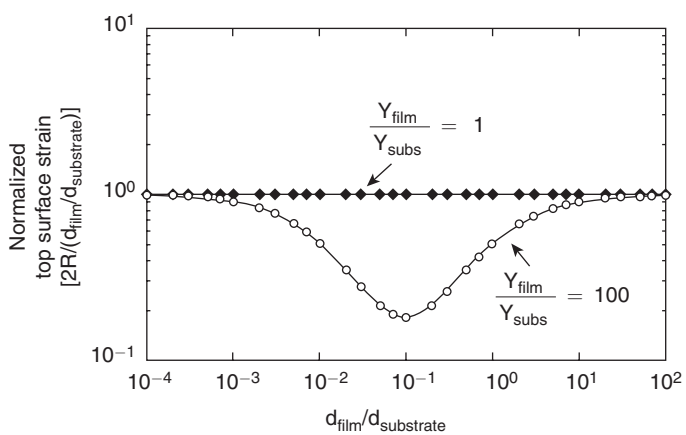

Figure 16.6 Normalized strain in the film as a function of film/substrate thickness ratio $d_{film}/d_{substrate}$ for two substrates: steel (ratio of Young's modulus $Y_{film}/Y_{subs} = 1$) and plastic ($Y_{film}/Y_{subs} = 100$). Reproduced with permission from [43].

$Y_{film}/Y_{substrate}$ equal to 1) and polymer (Young's modulus ratio equal to 100). For given radius of curvature (R in the figure) and film/substrate thickness ratio ($d_{film}/d_{substrate}$), the compliant substrate can reduce the strain by as much as a factor of 5 owing to the shift of the neutral axis toward the film.

Notice that the analytical models introduced in this chapter are accurate enough to determine the critical radius of curvature for thin flexible devices, for which the critical strain is $< 1–2$ % and R_{crit} is much greater than the total device thickness h. These models, however, are unable to capture mechanical nonlinearities associated with the geometry of actual devices (edge effects, thickness changes, etc.) and also with large displacements ($R_2 < 10$ hours, see e.g. [40]).

It is important to point out that R_{crit} is not a material property as it depends on substrate thickness. The key property is, again, the critical strain, which is controlled by the toughness of the brittle films, or by the toughness of the film/substrate interface as developed in Section 16.4.

16.4 Failure Mechanics of Brittle Films

As sketched in Figure 16.3 the film located on the top, convex side of the bend multilayer experiences tensile strains and the film located on the bottom, concave side of the bend multilayer experiences compressive strains. The magnitude of these strains depends on the applied curvature and on the internal strains. Failure occurs as soon as the strain in either film reaches the critical value ε_{crit} (tensile failure for the film on the top with formation of channeling cracks, and compressive failure for the film on the bottom with buckling and delamination). A clear and unambiguous analysis of the failure mechanisms of thin films requires identification of the *locus of failure*, i.e. whether the failure is cohesive (within a layer) or adhesive (at an interface between adjacent layers) [44]. The reader is also referred to the comprehensive fracture mechanics treatment in multilayers by [4].

16.4.1 Damage Phenomenology under Tensile and Compressive Loading

The failure process of brittle films on substrates under tensile loading reveals three damage stages depicted in Figure 16.7 [45].

Stage I: crack onset and random cracking (Figure 16.7a and d). Cracks initiate in the film at defect sites and start propagating perpendicular to the loading direction at a critical strain, ε_{crit} (also termed crack onset strain, COS). The interaction between cracks is negligible and the generation of new cracks is governed by the statistical distribution of defects within the film.

Stage II: mid-point cracking (Figure 16.7b and e). The crack density (CD) increases whereas the generation of new cracks diminishes. Transverse buckling with localized interfacial delamination is observed across fragments due to Poisson's ratio effects (visible in Figure 16.7c and f).

Stage III: delamination and saturation (Figure 16.7c and f). No further cracks are generated in this stage and CD reaches a saturation value, CD_{sat}, related to the so-called critical stress transfer length and interfacial shear strength [46]. Extensive transverse buckling is evident and delamination becomes the dominant failure mechanism.

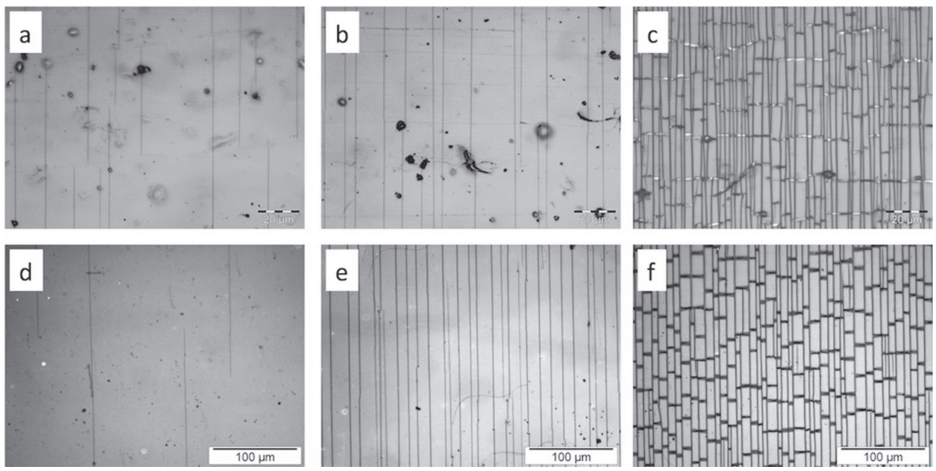

Figure 16.7 Optical micrographs of the fragmentation process of brittle films on polymer substrates under tensile loading (SiN_x on polyimide at (a): 1.2%, (b): 1.5%, and (c): 14.7% strain; ITO on PET at (d): 1.1%, (e): 2.2%, and (f): 11.6% strain). The scale bar in micrographs (a), (b), and (c) represents 20 µm.

Under compressive loading the dominant failure mode for films on substrates is buckling and associated adhesive failure at the film/substrate interface, with examples shown in Figure 16.8. Several morphologies can be observed such as the well-known "telephone cord" pattern [47] depending on the film thickness, in-plane stress state (uniaxial or biaxial), interfacial toughness, and film toughness. Detailed buckling analysis described next enables one to identify the source of problems and thereby to optimize the processing of the individual layers. For instance, the adhesion quality, and influences of processing steps, can be quantified, using the size of the buckle.

16.4.2 Experimental Methods

Two main methods are available to analyze the failure of brittle films, namely fragmentation in situ in a microscope (and related electro-fragmentation) for the tensile loading case and electro-bending, for both tensile and compressive loading cases. In a fragmentation test, a coated substrate is loaded under uniaxial tension, and the damage state in the film due to interfacial stress

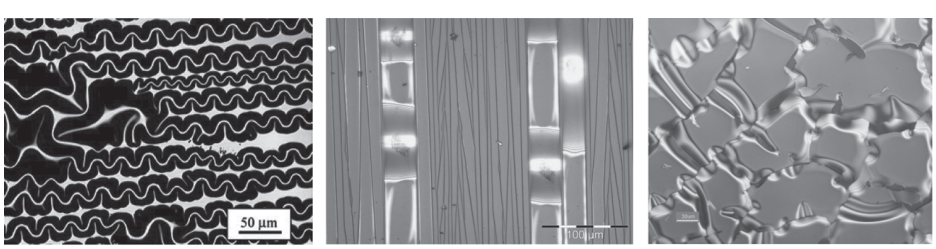

Figure 16.8 Buckling morphologies in films on substrates: (a) telephone cord buckling delamination of a compressed W film (reproduced with permission from [48]), (b) buckling in 800-nm-thick SiN_x fragments on polyimide under tensile stress due to lateral Poisson's contraction, and (c) buckling with and without cracks in a 400-nm-thick SiN_x film on polyimide (courtesy of Philips Research).

transfer from the substrate is analyzed as a function of strain. In-situ tests in an optical or scanning electron microscope are usually employed for the detection of cracks (e.g. Figure 16.6). The method is free of third-body interactions and is used to quantify the cohesive properties (which control critical strain) and the adhesive properties (which control delamination) of films on substrates [32, 49]. The fragmentation test is limited to high elongation substrates (i.e. with a strain to failure several times higher than that of the film). Electro-fragmentation tests carried out in situ (using special clamps to measure electrical resistance of the sample) enable correlating a macroscopic damage state variable (e.g. electrical resistance) to the actual damage at the microscopic scale [35]. Extension of such tests to dielectric films is possible with a conductive probe layer [50].

Bending test methods reproduce the loading state of flexed devices under quasi-static or cyclic loading conditions, using template cylinders of known radius [51,52], or through loading between two parallel plates [53]. This loading geometry is adequate to analyze the behavior of tensile loaded and compressed layers (i.e. layers located on the convex and concave sides of the bent multilayer, respectively). Bending tests are fast and are thus useful for statistical analyses of critical strain and for rapid screening of a series of materials. However, they are usually limited to conductive films, using electrical measurements as a signature of damage, since a direct observation of the damage state in situ in a microscope is hardly feasible. Again, extension of bending tests to dielectric films is possible with a conductive probe layer [54]. In the parallel plate geometry the sample curvature is not constant, with lowest radius of curvature and largest strain $\varepsilon_{\max} = 1.1985h/(L-h)$ in the middle of the bend, where h is the sample thickness and L is the distance between the two plates [55].

16.4.3 Fracture Mechanics Analysis

The cohesive properties of the film (critical strain, toughness, Weibull modulus) are derived from the early stages of tensile failure (initiation stage I) [46, 56–60]. The film toughness G_{coh} can be calculated assuming that it is equal to the energy release rate at critical strain [61–63]. For a semi-infinite substrate one has:

$$G_{coh} = \frac{\pi}{2} h_f \bar{E}_f \varepsilon_{crit}^2 g\left(\alpha_D, \beta_D\right) \tag{16.10}$$

where h_f and $\overline{E_f} = E_f/\left(1-V_f^2\right)$ are the thickness and plane strain modulus of the film (E_f and ν_f are the Young's modulus and Poisson's ratio of the film) and $g\left(\alpha_D, \beta_D\right)$ is a function of the Dundurs parameters α_D and β_D [64], which describe the elastic mismatch of the film/substrate system. In the case of plane strain problems:

$$\alpha_D = \frac{\bar{E}_f - \bar{E}_s}{\bar{E}_f + \bar{E}_s} \quad \text{and} \quad \beta_D = \frac{\mu_f\left(1-2\nu_s\right) - \mu_s\left(1-2\nu_f\right)}{2\mu_f\left(1-\nu_s\right) + 2\mu_s\left(1-\nu_f\right)} \tag{16.11}$$

where $\overline{E_s} = E_s/\left(1-V_s^2\right)$ is the plane strain modulus of the substrate (E_s and ν_s are the Young's modulus and Poisson's ratio of the substrate), and $\mu = E_f/\left(2+2V_f\right)$ and $\mu_s = E_s/\left(2+2V_s\right)$ are the shear moduli of the film and substrate, respectively. For films with the same properties as their substrate, $\alpha_D = \beta_D = 0$. A stiff film on a soft substrate results in α - 1, whereas a soft film on a stiff substrate results in α_D - –1. The function g is primarily dependent on parameter α_D, which

is therefore more representative of film/substrate elastic contrast than parameter β_D. For most film/substrate combinations $0 < \beta_D < \alpha_D/4$.

A practical consequence of Equation 16.10 is that the critical strain for film failure scales with the inverse of square root of film thickness and elastic contrast (providing that the elastic modulus and toughness of the film are independent of film thickness). It was, for example, found that the critical strain for silica films on a steel substrate was a factor of almost five times higher than on a polymer substrate [65]. This huge difference in critical strain was largely due to the difference in elastic contrast, and also to different internal strains. Reducing film thickness or film/substrate elastic contrast both lead to an increase in critical strain, hence increasing the admissible curvature of the multilayer device. For substrates of finite thickness, Equation 16.10 remains accurate when the substrate to film stiffness ratio $\overline{E}_s h_s = E_f h_f > 10$, otherwise the approximation devised by [65] may be used.

The interfacial toughness is obtained from an energy release rate analysis for steady-state tunneling delamination and buckling, again assuming that it is equal to the energy release rate at critical (buckling) strain:

$$G_{adh} = \frac{\overline{E}_f \varepsilon^2 h_f}{2}\left(1 - \frac{\varepsilon_{crit}}{\varepsilon}\right)^2 f\left(\Psi;\alpha_D;\beta_D\right) \tag{16.12}$$

where ε is the applied compressive strain and $f\left(\Psi;\alpha_D;\beta_D\right)$ is a function of mode-mixity ψ and Dundurs parameters. Notice that Equation 16.12 is valid for buckling without film cracking. The case where cracking occurs is treated in [66]. Explicit relations between the adhesion energy and the buckle morphology were developed in [67]. An alternative based on the analysis of edge delamination in a fragmentation experiment is treated in [68].

16.4.4 Role of Internal Stresses

In the presence of internal stresses, the measured critical strain is a linear combination of an intrinsic failure strain, ε^*_{crit}, and the internal strain, ε_i:

$$\varepsilon_{crit} = \varepsilon^*_{crit} - \varepsilon_i \tag{16.13}$$

The analysis of internal strains thus enables determination of the intrinsic failure strain of the film. An alternative electromechanical method was proposed to directly obtain these two strains simultaneously [69]. The knowledge of the various contributions to the actual critical strain of a film on a substrate can be useful to optimize both film composition (and associated intrinsic strain) and processing conditions (and associated internal strain). Large internal tensile strains may lead to premature cracking if the film is loaded in tension. On the contrary large internal compressive strains combined with insufficient adhesion are often the cause of buckling failure [47, 70]. Further details are given in [71], where the authors emphasize the importance of increasing interfacial adhesion and decreasing film/substrate elastic contrast to compensate for the presence of internal compressive strains and prevent premature occurrence of buckling failure.

16.4.5 Influence of Film Thickness on Critical Strain

Figure 16.9 regroups fragmentation data for silicon nitride and silicon oxide films with different thickness [72] and shows the relevance of Equation 16.10 to predict the influence of film thickness on critical strain. It is evident that the fragmentation technique is very sensitive: thicker films crack at a lower strain, and their crack density at saturation is lower. Notice that this behavior is quite different from

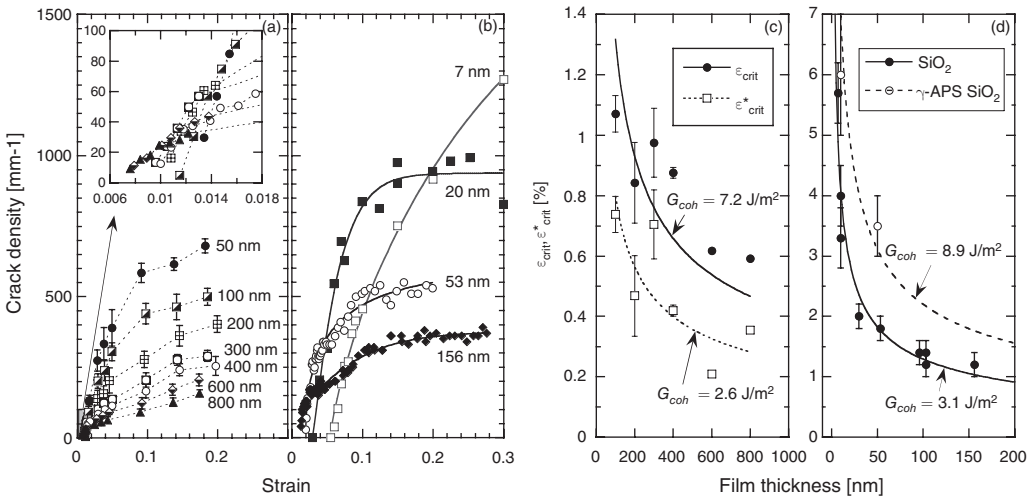

Figure 16.9 Fragmentation process of SiN_x films on polyimide ((a) the film thickness is indicated; the inset shows the early fragmentation stage) and SiO_2 films on PET ((b) the film thickness is indicated), and critical strain versus film thickness for the SiN_x films (c) and SiO_2 and silylated SiO_2 films (d). The lines in (c) and (d) represent the fracture mechanics scaling (Equation 16.10) with best fit values of G_{coh} indicated.

that of thin metal films due to absence of yielding [73]. The toughness G_{coh} of the two materials is indicated in Figure 16.9c and d. In the case of the SiN_x films with significant compressive stresses [72], the toughness was found to be equal to 7.2 J/m^2 (using ε_{crit} data) or 2.6 J/m^2 (using ε^*_{crit} data, i.e. correcting for the presence of internal stresses). This marked difference resulting from the presence of compressive stresses in SiN_x films was confirmed using nanoindentation [74]. In the case of the SiO_2 films the toughness was found to be equal to 3.1 J/m^2, a typical value for fused silica [75]. Modification of the OH-terminated SiO_2 surface with organo-silane molecules (γ-APS) enabled a threefold increase the toughness of the film, resulting in significant increase of critical strain [76–78].

16.5 Durability Influences

16.5.1 Influence of Temperature

Increasing the temperature impacts the critical strain of films due to the combined action of substrate softening and expansion behavior on heating [79, 80]. The former effect increases Dundurs parameter α_D and elastic contrast function g, leading to a decrease of ε_{crit} (Equation 16.10). The latter generates tensile thermal strains in the film (Equation 16.2a, the CTE of polymer substrates is generally higher than that of inorganic films), also contributing to a decrease of ε_{crit}. Figure 16.10 shows the considerable influence of temperature on critical strain of an oxide film on a PET substrate. The temperature dependence of ε^*_{crit} and ε_i is also shown. Upon heating from room temperature to 140°C ε_{crit} decreased from 0.5% to 0.2%. Such 0.3% decrease was controlled by the 0.1% decrease of ε^*_{crit} due to substrate softening and the 0.2% increase of tensile strain ε_i. Further increasing the temperature to 180°C led to an unexpected increase of ε_{crit} back to 0.5% at 180°C. This was essentially due to shrinkage of the polymer substrate (evaporation of residual water and relaxation of process-induced molecular orientation) and corresponding buildup of compressive strain in the film.

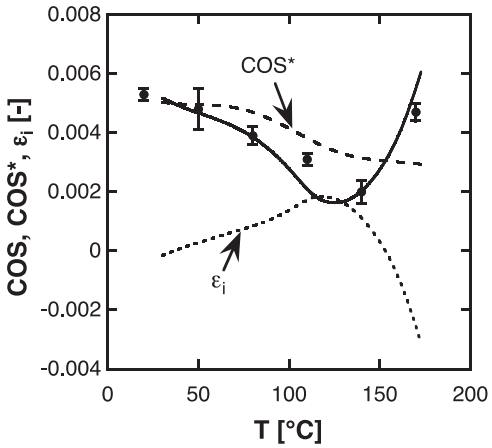

Figure 16.10 Predicted ε_{crit} (COS, solid line) versus measured ε_{crit} (dots) as a function of temperature for 209-nm-thick silicon oxide films on a PET substrate. Internal strain ε_i and ε^*_{crit} (COS*) predictions are also shown. Reproduced with permission from [79].

Additional temperature influences relate to the viscoelastic nature of polymer substrates, which may manifest itself through relaxation and creep phenomena, i.e. problems of dimensional stability. Not much effort has been made on this issue, for which numerical simulation tools could be powerful to design devices with improved stability.

16.5.2 Fatigue

The critical strain for film failure determined under quasi-static loading [49, 53] might not be representative of the actual loading present during operational life. In fact, evidence of slow crack growth was reported for indium tin oxide (ITO) films under fatigue loading at strain levels below the critical strain [81, 82]. High cycle fatigue of thin films on polymer substrates has been studied in detail for metallic films (especially Cu and Al) [83–87] and transparent conductive oxide films [52, 88]. Figure 16.11 shows the peculiar damage morphology of tensile fatigue loaded ITO films on polyester substrates, where tensile cracks and edge delamination are evident. The extensive

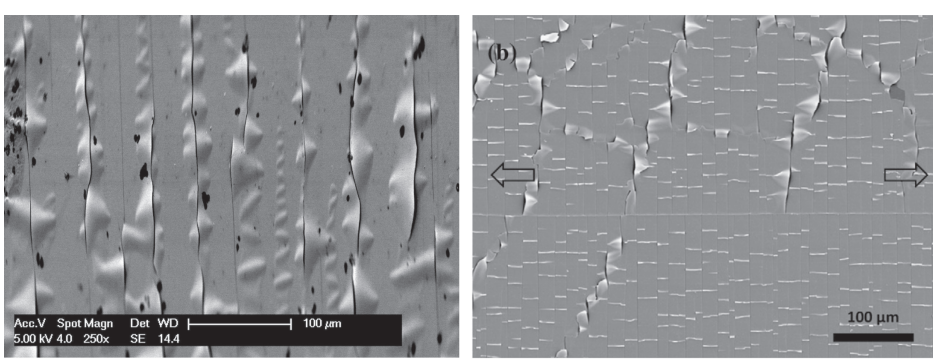

Figure 16.11 Electron micrographs of damage state in ITO films on PET (tensile fatigue loaded to 100′000 cycles at 0.58% strain amplitude, left) and PEN (immersed in 0.1 M acid and tensile tested to 20% strain, right. Reproduced with permission from [90].

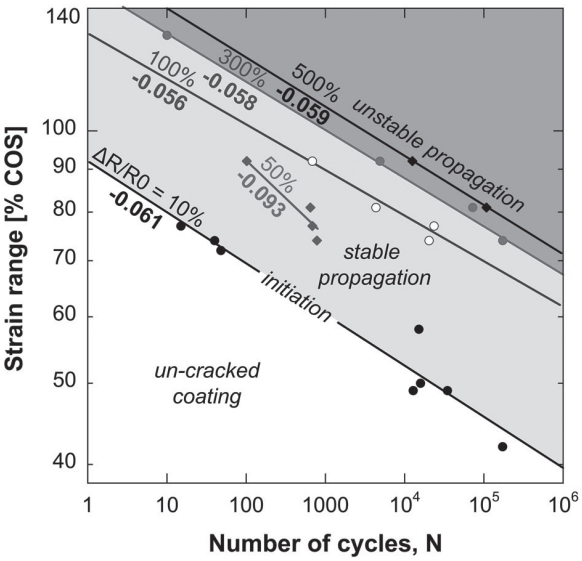

Figure 16.12 Fatigue damage map of a TCO coating tested under cyclic loading to predefined strain levels (normalized with respect to the critical strain, COS). Reproduced with permission from [35]. The lines are power law fits to the experimental data for selected resistance increase $\Delta R/R_0$ levels (indicated in percentages in the figure together with the fatigue strength exponents).

edge delamination is the sign of damage accumulation. It was reported that fatigue under compressive loading is more critical than under tensile loading, which may be a result of compressive residual stresses [89].

Figure 16.12 shows a fatigue endurance map of a TCO coating on a PET substrate [35], where iso-resistance levels are shown versus number of cycles and maximum strain. Initiation of tensile cracks corresponded to a change of electrical resistance $\Delta R/R_0 = 10\%$, where R and R_0 are the resistances of the strained and unstrained samples, respectively. Stable propagation occurred until $\Delta R/R_0 \sim 300\%$ after which catastrophic failure took place. The same power-law scaling with a fatigue strength exponent equal to -0.06 was found between maximum strain and critical number of cycles for both initiation and propagation of tensile cracks. The present scaling follows the modified Basquin law for non-zero mean stress [91], which enables predicting damage events in such coatings upon fatigue loading to any strain levels. For instance, at maximum strain equal to 70% of the critical strain, cracks will initiate after ca. 70 cycles. They will progressively grow upon further cycling until catastrophic failure, which will occur after ca. 800 000 cycles. The existence of a threshold strain was not investigated. It would be $< 40\%$ of the critical strain and would correspond to an endurance limit well beyond 10^5 cycles for this TCO coating.

16.5.3 Corrosion

The presence of corrosive environments (moisture, acids, bases) has been reported to negatively impact the mechanical integrity of inorganic films on polymers. Moisture plays a significant role in film delamination due to interfacial diffusion and reduction of interfacial toughness, combined with buildup of hygroscopic strains in the polymer substrate [92]. Oxide

films may also corrode when exposed to moisture [93], acids, and bases, the corrosion state being controlled by the pH as described in the form of *Pourbaix diagrams* [94], eventually decreasing the critical strain for tensile failure and increasing the rate of crack growth [90]. Corroding environments and tensile mechanical stresses exacerbate each other to initiate and propagate cracks, a phenomenon known as *stress corrosion cracking* (SCC). SCC is controlled by microscopic processes occurring at crack tips, characterized by high concentrations of corroding medium. Acrylic acid such as that found in pressure-sensitive adhesives causes cracks to initiate at strains as low as a quarter of those observed for films with no corrosion [95]. As shown in Figure 16.13, the combination of fatigue and corrosion severely reduces the critical strain for tensile failure of ITO films and speeds up the degradation of the electrical conductivity under cyclic loading [96].

In real life multiple degradation factors (temperature, moisture, mechanical, and electrical stresses) often act simultaneously and in synergy. Only limited data are available to understand these coupled phenomena and it would thus be useful to increase knowledge on the resulting lifetime of display devices. Inspiring approaches to this end are presented in the Duracosys conference series, primarily devoted to structural fiber reinforced polymer composites, indeed with similar time-dependent degradation features to the present flexible composite devices ([97] and following years).

Prevention of SCC follow three main principles: (i) decrease the tensile stress (internal and applied) through process and multilayer optimization, (ii) reduce the pH of the corroding medium, and (iii) improve the composition of the (oxide) film or use passivation layers. As pointed out in Section 16.4.5, controlled corrosion of a silica gas barrier film combined with crosslinking of an aminosilane passivation layer enabled tremendous improvement of both the critical strain for tensile failure and the barrier performance of the silica film [76, 77]. The key was the healing of crack initiation defects in the oxide resulting from the dissolution of superficial layers [98, 99].

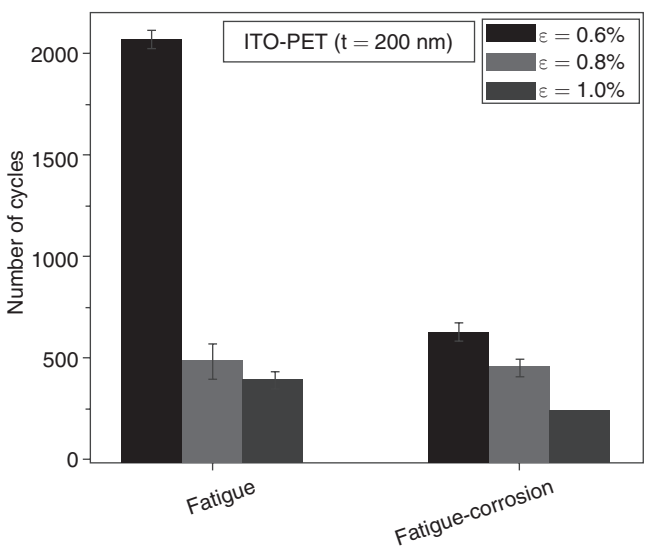

Figure 16.13 Critical number of cycles for fatigue and fatigue corrosion with acrylic acid of 200-nm-thick ITO-coated PET films. Reproduced with permission from [96].

16.6 Toward Robust Layers

Much effort is being paid to develop unbreakable flexible devices, either by adequate designs to prevent premature failure of brittle device components or by the substitution of fragile layers by robust ones. Design approaches are implemented to reduce film strain, such as neutral axis designs (Equation 16.7). The idea is to place the brittle film at the neutral axis, using an additional layer on the opposite side to the substrate, with appropriate thickness and Young's modulus [43]. In this case negligible strain will build up in the film upon bending the multilayer assembly. The critical radius of curvature will no longer be controlled by the critical strain of the film, but rather by delamination problems. Other designs relevant for brittle films are in the form of wavy patterns, which are able to accommodate tensile strains considerably larger than the intrinsic critical strain of the film [100, 101].

Robust layers include films with improved fracture toughness, controlled compressive internal stresses, as well as reduced thickness (see Section 16.4.5). Examples are multilayer structures, which combine several of the aforementioned factors. In the case of ITO films, the additions of Ti [102] and Ag [103] interlayers were reported to improve the crack and delamination resistances of the films, owing to an increase of the crystallinity of the ITO. Such efforts may benefit from numerical analyses of the influence of interlayer toughness and thickness on the critical strain of the film [104]. Planarization "hard coats" reduce the film/substrate elastic contrast and enable significant increase of the critical strain of ITO films [105]. Research is also extremely active to substitute fragile layers by intrinsically compliant layers. Graphene, with a strain to failure of 13% [106] provides an unbreakable alternative to ITO [107]. Further examples include semi-transparent Cu nanowire meshes [108] and Ag grids embedded in PEDOT-PSS [109]. Last but not least, self-healing materials with the ability of autonomous damage recovery emerge as new challenging perspectives for the development of robust functional nanosystems [110,111]. Self-healing encapsulation of light-emitting diodes [112], self-healing gate dielectrics in flexible graphene field-effect transistors [113], and self-healing Ag interconnects [114, 115] are recent examples of such developments relevant for flexible display technologies.

16.7 Final Remarks

The allowable radius of curvature of flexible displays is limited by mechanical failures, such as cohesive cracking of functional films and interfacial delamination between adjacent device layers. Cohesive failure occurs predominantly under tensile loading, with critical failure strain usually close to 1%. Buckling delamination results from compressive loading and insufficient adhesion, and may also initiate around 1% strain. In both tensile and compressive modes, the corresponding critical radius of curvature is of the order of few cm, for display thickness of few 100 μm.

Adequate designs should be based on knowledge of critical strains, internal stress state, and a number of material properties. A variety of methods have been developed to this end, such as the electro-fragmentation and electro-fatigue tests in situ in a microscope. These two methods reproduce the thermomechanical loads present during processing and service life, hence they enable identifying and modeling the critical conditions for failure. In fact, critical strains were reported to decrease with time under e.g. fatigue and SCC conditions, which ultimately limits the flexibility of the display. Possible degradation processes are multiple and often act in synergy, and further research on the long-term endurance of flexible display multilayers is advisable. Together

with continuous improvements in mechanical models, numerical simulations and test methods, novel designs, improved fabrication processes, and emergence of new materials with increased mechanical robustness, improved knowledge on degradation processes will be key for the manufacturing of truly reliable flexible displays.

Acknowledgments

The author is indebted to Piet Bouten for nanoindentation tests and fruitful discussions. He would like to thank Gil Rochat, Léonard Médico, Fabio Demarco, Gregory Tornare, Pierre Dumont, Damien Gilliéron, Albert Pinyol, and Judith Waller for experimental support.

Nomenclature

a_0, a_1	Constants in strain profile (Equation 16.6).
CD, CD_{sat}	Crack density, crack density at saturation
CHE	Coefficient of hygroscopic expansion
CTE	Coefficient of thermal expansion
E, E_f, E_s	Young's modulus, of film, of substrate
ε^*_{crit}, $\overline{E}_f$	Plane strain moduli of film, of substrate
$g(\alpha';\beta')$	Normalized energy release rate
G_{coh}, G_{adh}	Film toughness, interfacial toughness
h, h_f, h_s	Thicknesses of multilayer, of film, of substrate
R, R_0	Electrical resistance, of unstrained film
R_1, R_2	Radii of curvature of substrate, of coated substrate
R_{crit}	Critical radius of curvature
RH	Relative humidity
SCC	Stress corrosion cracking
T	Temperature
TCO	Transparent conducting oxide
w	Indentation depth function (Equation 16.1)
α_D, β_D	Dundurs parameters
α_s, α_f	CTE of substrate, of film
β_s, β_f	CHE of substrate, of film
χ	Film-to-substrate Young's modulus ratio
ε	Strain
ε_{crit}, COS	Critical failure strain, crack onset strain
ε_{crit}	Intrinsic crack onset strain
ε_i	Film internal strain
$\overline{E}_s$ ε_i^{in}, ε_i^{th}, ε_i^{hy}	Intrinsic, thermal, hygroscopic contributions to the internal strain

ν, ν_f, ν_s	Poisson's ratio of multilayer, of film, of substrate
η	Film-to-substrate thickness ratio
μ_f, μ_s	Shear modulus of film, of substrate
α	Mode-mixity
ξ	Adjustable factor in nanoindentation tests

References

1 Crawford, G.P. (2005). *Flexible Flat Panel Displays*. Chichester: John Wiley & Sons.

2 Nathan, A., Ahnood, A., Cole, M.T., Lee, S., Suzuki, Y., Hiralal, P., Bonaccorso, F. et al. (2012). Flexible electronics: The next ubiquitous platform. *Proc. IEEE* 100: 1486–1517.

3 Leterrier, Y., Pinyol, A., Dumont, P., Gillieron, D., Mewani, V., Manson, J.A., Andersons, J., Bouten, P., Timmermans, P. et al. (2008). Invited paper: Models and experiments of mechanical integrity for flexible displays. *SID Sympos. Digest Tech. Papers* 39: 310–313.

4 Hutchinson, J.W. and Suo, Z. (1992). *Adv. Appl. Mech.* 29: 63–191.

5 MacDonald, W.A., Looney, M.K., MacKerron, D., Eveson, R., and Rakos, K. (2008). Designing and manufacturing substrates for flexible electronics. *Plast. Rubber Compos.* 37: 41.

6 Park, J.S., Chae, H., Chung, H.K., and Lee, S.I. (2011). Thin film encapsulation for flexible AM-OLED: A review. *Semicond. Sci. Technol.* 26.

7 Gokhale, A.A. and Lee, I. (2014). Recent advances in the fabrication of nanostructured barrier films. *J. Nanosci. Nanotechnol.* 14: 2157.

8 Szyszka, B., Dewald, W., Gurram, S.K., Pflug, A., Schulz, C., Siemers, M., Sittinger, V. and Ulrich, S. (2012). Recent developments in the field of transparent conductive oxide films for spectral selective coatings, electronics and photovoltaics. *Curr. Appl. Phys.* 12: S2–S11.

9 Wang, P.-C., Dewald, W., Gurram, S.K., Pflug, A., Schulz, C., Siemers, M., Sittinger, V. and Ulrich, S. (2013). Transparent electrodes based on conducting polymers for display applications. *Displays* 34: 301.

10 Fortunato, G., Pecora, A., and Maiolo, L. (2012). Polysilicon thin-film transistors on polymer substrates. *Mater. Sci. Semicond. Process.* 15: 627.

11 Fortunato, E., Barquinha, P., and Martins, R. (2012). Oxide semiconductor thin-film transistors: A review of recent advances. *Adv. Mater.* 24: 2945.

12 Bull, S.J. (2005). Nanoindentation of coatings. *J. Phys. D: Appl. Phys.* 38: R393.

13 Sun, Y.J., Padbury, R.P., Akyildiz, H.I., Goertz, M.P., Palmer, J.A., and Jur, J.S. (2013). Influence of Subsurface hybrid material growth on the mechanical properties of atomic layer deposited thin films on polymers. *Chem. Vapor Depos.* 19: 134.

14 Chang, R.-C., Tsai, F.-T., and Tu, C.-H. (2013). A direct method to measure the fracture toughness of indium tin oxide thin films on flexible polymer substrates. *Thin Solid Films* 540: 118.

15 Kassavetis, S., Logothetidis, S., and Zyganitidis, I. (2012). Nanomechanical testing of the barrier thin film adhesion to a flexible polymer substrate. *J. Adhes. Sci. Technol.* 26: 2393.

16 Chalker, P.R., Bull, S.J., and Rickerby, D.S. (1991). A review of the methods for the evaluation of coating-substrate adhesion. *Mater. Sci. Eng.* A140: 583.

17 Pharr, G.M. and Oliver, W.C. (1992). Measurement of thin film mechanical properties using nanoindentation. *MRS Bull.* July: 28–33.

18 Oliver, W.C. and Pharr, G.M. (2004). Measurement of hardness and elastic modulus by instrumented indentation: Advances in understanding and refinements to methodology. *J. Mater. Res.* 19: 3.

19 Doerner, M.F. and Nix, W.D. (1986). A method for interpreting the data from depth-sensing indentation instruments. *J. Mater. Res.* 1: 601.

20 Bhushan, B. and Li, X.D. (2003). Nanomechanical characterisation of solid surfaces and thin films. *Int. Mater. Rev.* 48: 125.

21 Fischer-Cripps, A.C. (2006). Review of analysis and interpretation of nanoindentation test data. *Surf. Coat. Technol.* 200: 4153.

22 Reddy, J.R. (2004). *Mechanica of Laminated Composite Plate and Shells: Theory and Analysis*. Boca Raton: CRC Press.

23 Hahm, S.W., Hwang, H.S., Kim, D., and Khang, D.Y. (2009). Buckling-based measurements of mechanical moduli of thin films. *Electron. Mater. Lett.* 5: 157.

24 Tahk, D., Lee, H.H., and Khang, D.Y. (2009). Elastic moduli of organic electronic materials by the buckling method. *Macromolecules* 42: 7079.

25 Cuberes, M.T., Assender, H.E., Briggs, G.A.D., and Kolosov, O.V. (2000). Heterodyne force microscopy of PMMA/rubber nanocomposites: Nanomapping of viscoelastic response at ultrasonic frequencies. *J. Phys. D-Appl. Phys.* 33: 2347.

26 Wittkowski, T., Jorzick, J., Seitz, H., Schroder, B., Jung, K., and Hillebrands, B. (2001). Elastic properties of indium tin oxide films. *Thin Solid Films* 398: 465.

27 Lefeuvre, O., Kolosov, O.V., Every, A.G., Briggs, G.A.D., and Tsukahara, Y. (2000). Elastic measurements of layered nanocomposite materials by brillouin spectroscopy. *Ultrasonics* 38: 459.

28 Rochat, G., Leterrier, Y., Plummer, C.J.G., Månson, J.-A.E., Szoszkiewicz, R., Kulik, A.J., and Fayet, P. (2004). Effect of substrate crystalline morphology on adhesion of PECVD thin SiOx coatings on polyamide. *J. Appl. Phys.* 95: 5429.

29 Ohring, M. (1992). *The Materials Science of Thin Films*. New-York: Academic Press.

30 Tamulevicius, S. (1998). Stress and strain in the vacuum-deposited thin films. *Vacuum* 51: 127.

31 Spaepen, F. (2000). Interfaces and stresses in thin films. *Acta Mater.* 48: 31.

32 Leterrier, Y. (2003). Durability of nanosized gas barrier coatings on polymers. *Prog. Mater. Sci.* 48: 1.

33 Dumont, P., Tornare, G., Leterrier, Y., and Månson, J.-A.E. (2007). Intrinsic, thermal and hygroscopic residual stresses in thin gas-barrier films on polymer substrates. *Thin Solid Films* 515: 7437.

34 Leterrier, Y., Wyser, Y., and Månson, J.A.E. (2001). Internal stresses and adhesion of thin silicon oxide coatings on poly(ethylene terephthalate). *J. Adhes. Sci. Technol.* 15: 841.

35 Leterrier, Y., Mottet, A., Bouquet, N., Gillieron, D., Dumont, P., Pinyol, A., Lalande, L., Waller, J.H., and Manson J.A.E. (2010). Mechanical integrity of thin inorganic coatings on polymer substrates under quasi-static, thermal and fatigue loadings. *Thin Solid Films* 519: 1729.

36 Noyan, I.C., Huang, T.C., and York, B.R. (1995). Residual-stress strain analysis in thin-films by x-ray-diffraction. *Crit. Rev. Solid State Mater. Sci.* 20: 125.

37 Withers, P.J. and Bhadeshia, H. (2001). Overview – Residual stress part 1 – Measurement techniques. *Mater. Sci. Technol.* 17: 355.

38 Stoney, G.G. (1909). The tension of metallic films deposited by electrolysis. *Proc. Roy. Soc. London* a82.

39 Röll, K. (1976). Analysis of stress and strain distribution in thin films and substrates. *J. Appl. Phys.* 47: 3224.

40 Masters, C.B. and Salamon, N.J. (1993). Geometrically nonlinear stress deflection relations for thin-film substrate systems. *Int. J. Eng. Sci.* 31: 915.

41 Sasabayashi, T., Ito, N., Nishimura, E., Kon, M., Song, P.K., Utsumi, K., Kaijo, A., and Shigesato, Y. (2003). Comparative study on structure and internal stress in tin-doped indium oxide and indium-zinc oxide films deposited by r.f. magnetron sputtering. *Thin Solid Films* 445: 219.

42 Fang, W.L. and Lo, C.Y. (2000). On the thermal expansion coefficients of thin films. *Sens. Actuat. Phys.* 84: 310.

43 Suo, Z., Ma, E.Y., Gleskova, H., and Wagner, S. (1999). Mechanics of rollable and foldable film-on-foil electronics. *Appl. Phys. Lett.* 74: 1177.

44 Pitton, Y., Hamm, S.D., Lang, F.-R., Leterrier, Y., Mathieu, H.J., and Månson, J.-A.E. (1995), An adhesion study of SiOx/PET films: A comparison between scratch and fragmentation tests, 1st ICAST, Amsterdam, Holland, October 16–20.

45 Wheeler, D.R. and Osaki, H. (1990). Intrinsic bond strength of metal-films on polymer substrates - a new method of measurement. *ACS Sympos. Ser.* 440: 500.

46 Leterrier, Y., Boogh, L., Andersons, J., and Månson, J.-A.E. (1997). Adhesion of silicon oxide layers on poly(ethylene terephthalate). I: Effect of substrate properties on coating's fragmentation kinetics. *J. Polym. Sci. B: Polym. Phys* 35: 1449.

47 Moon, M.W., Jensen, H.M., Hutchinson, J.W., Oh, K.H., and Evans, A.G. (2002). The characterization of telephone cord buckling of compressed thin films on substrates. *J. Mech. Phys. Solids* 50: 2355.

48 Volinsky, A.A. and Waters, P. (2013). Delaminated film buckling microchannels. In: *Mechanical Self-Assembly 2013: Science and Applications* (Ed. X. Chen), 153–170. New York: Springer.

49 Plojoux, J., Leterrier, Y., Månson, J.-A.E., and Templier, F. (2007). Mechanical integrity analysis of multilayer insulator coatings on flexible steel substrates. *Thin Solid Films* 515: 6890.

50 Pinyol, A., Meylan, B., Gilliéron, D., Mewani, V., Leterrier, Y., and Månson, J.A.E. (2009). Electro-fragmentation analysis of dielectric thin films on flexible polymer substrates. *Thin Solid Films* 507: 2007.

51 Grego, S., Lewis, J., Vick, E., and Temple, D. (2005). Development and evaluation of bend-testing techniques for flexible-display applications. *J. Soc. Inf. Disp.* 13: 575.

52 Cairns, D.R. and Crawford, G.P. (2005). Electromechanical properties of transparent conducting substrates for flexible electronic displays. *Proc. IEEE* 93: 1451.

53 Abdallah, A.A., Kozodaev, D., Bouten, P.C.P., den Toonder, J.M.J., Schubert, U.S., and de With, G. (2006). Buckle morphology of compressed inorganic thin layers on a polymer substrate. *Thin Solid Films* 503: 167.

54 Guan, Q., Laven, J., Bouten, P.C.P., and De With, G. (2013). Subcritical crack growth in SiNx thin-film barriers studied by electro-mechanical two-point bending. *J. Appl. Phys.* 113.

55 Matthewson, M.J., Kurkjian, C.R., and Gulati, S.T. (1986). Strength measurement of optical fibers by bending. *J. Am. Ceram. Soc.* 69: 815.

56 Leterrier, Y., Andersons, J., Pitton, Y., and Månson, J.-A.E. (1997). Adhesion of silicon oxide layers on poly(ethylene terephthalate). II: Effect of coating thickness on adhesive and cohesive strengths. *J. Polym. Sci. B: Polym. Phys* 35: 1463.

57 Hui, C.Y., Shia, D., and Berglund, L.A. (1999). Estimation of interfacial shear strength: An application of a new statistical theory for single fiber composite test. *Compos. Sci. Technol.* 59: 2037.

58 Nairn, J.A. (2000). Matrix microcracking in composites. In: *Comprehensive Composite Materials, Vol. 2. Polymer-Matrix Composites* (ed. A. Kelly and C. Zweben), 403–432. Oxford: Elsevier.

59 Kim, S.R. and Nairn, J.A. (2000). Fracture mechanics analysis of coating/substrate systems Part I: Analysis of tensile and bending experiments. *Eng. Fract. Mech.* 65: 573.

60 Ochiai, S., Iwamoto, S., Nakamura, T., and Okuda, H. (2007). Crack spacing distribution in coating layer of galvannealed steel under applied tensile strain. *ISIJ Int.* 47: 458.

61 Beuth, J.L. (1992). Cracking of thin bonded films in residual tension. *Int. J. Solids Struct.* 29: 1657.

62 Ambrico, J.M. and Begley, M.R. (2002). The role of initial flaw size, elastic compliance and plasticity in channel cracking of thin films. *Thin Solid Films* 419: 144.

63 Andersons, J. et al. (2008). Evaluation of toughness by finite fracture mechanics from crack onset strain of brittle coatings on polymers. *Theor. Appl. Fract. Mech.* 49: 151.

64 Dundurs, J. (1969). Edge-bonded dissimilar orthogonal elastic wedges. *J. Appl. Mech.* 36: 650.

65 Leterrier, Y., Pinyol, A., Gillieron, D., Manson, J.A.E., Timmermans, P.H.M., Bouten, P.C.P., and Templier, F. (2010). Mechanical failure analysis of thin film transistor devices on steel and polyimide substrates for flexible display applications. *Eng. Fract. Mech.* 77: 660.

66 Cotterell, B. and Chen, Z. (2000). Buckling and cracking of thin films on compliant substrates under compression. *Int. J. Fract.* 104: 169.

67 Cordill, M.J., Fischer, F.D., Rammerstorfer, F.G., and Dehm, G. (2010). Adhesion energies of Cr thin films on polyimide determined from buckling: Experiment and model. *Acta Materialia* 58: 5520.

68 Tarasovs, S., Andersons, J., and Leterrier, Y. (2010). Estimation of interfacial fracture toughness based on progressive edge delamination of a thin transparent coating on a polymer substrate. *Acta Materialia* 58: 2948.

69 Vellinga, W.P., De Hosson, J.T.M., and Bouten, P.C.P. (2011). Direct measurement of intrinsic critical strain and internal strain in barrier films. *J. Appl. Phys.* 110.

70 Evans, A.G., Drory, M.D., and Hu, M.S. (1988). The cracking and decohesion of thin-films. *J. Mater. Res.* 3: 1043.

71 Bouten, P.C.P., Leterrier, Y., and Slikkerveer, P.J. (2005). *Flexible Flat Panel Displays* (Ed. G.P. Crawford). New-York: Wiley.

72 Andersons, J., Leterrier, Y., Tornare, G., Dumont, P., and Månson, J.-A.E. (2007). Evaluation of interfacial stress transfer efficiency by coating fragmentation test. *Mech. Mater.* 39: 834.

73 Lu, N., Suo, Z., and Vlassak, J.J. (2010). The effect of film thickness on the failure strain of polymer-supported metal films. *Acta Materialia* 58: 1679.

74 King, S., Chu, R., Xu, J., and Huening, J. (2009). Impact of film stress on nanoidentation fracture toughness measurements for PECVD SiNx:H films. *ECS Trans.* 19: 455.

75 Freiman, S.W. (1980). Fracture mechanics of glass. In : *Glass Science and Technology, Vol 5, Elasticity and Strength of Glasses* (ed. D.R. Uhlmann and N.J. Kreidl). New York: Academic Press.

76 Bouchet, J., Rochat, G., Leterrier, Y., Månson, J.-A.E., and Fayet, P. (2006). The role of the amino-organosilane/SiOx interphase in the barrier and mechanical performance of nanocomposites. *Surf. Coat. Technol.* 200: 4305.

77 Singh, B., Bouchet, J., Leterrier, Y., Manson, J.A.E., Rochat, G., and Fayet, P. (2007). Durability of aminosilane-silica hybrid gas-barrier coatings on polymers. *Surf. Coat. Technol.* 202: 208.

78 Leterrier, Y., Singh, B., Bouchet, J., Månson, J.-A.E., Rochat, G., and Fayet, P. (2009). Supertough UV-curable silane/silica gas barrier coatings on polymers. *Surf. Coat. Technol.* 203: 3398.

79 Waller, J.H., Lalande, L., Leterrier, Y., and Månson, J.-A.E. (2011). Modelling the effect of temperature on crack onset strain of brittle coatings on polymer substrates. *Thin Solid Films* 519: 4249.

80 Hu, K., Cao, Z.H., Wang, L., She, Q.W., and Meng, X.K. (2013). The anomalous temperature effect on the ductility of nanocrystalline Cu films adhered to flexible substrates. *Chin. Phys. Lett.* 30.

81 Pinyol, A., Meylan, B., Gilliéron, D., Mottet, A., Mewani, V., Leterrier, Y., and Månson, J.-A.E. (2008). Electro-fragmentation analysis of dielectric thin films on flexible polymer substrates. In: *Large-Area Processing and Patterning for Active Optical and Electronic Devices (Mater. Res. Soc. Symp. Proc. Volume 1030E, Warrendale, PA, 2008), 1030-G03-12* (ed. -S.C.-S.V. Buloviæ, I. Kymissis, J. Rogers, M. Shtein, and T. Someya).

82 Oh, J.S., Cho, Y.R., Cheon, K.E., Karim, M.A., and Jung, S.J. (2007). Failure mechanism of patterned ITO electrodes on flexible substrate under static and dynamic mechanical stresses. *Sol. State Phenom.* 124-126: 411.

83 Martynenko, E., Zhou, W., Chudnovsky, A., Li, R.S., and Poglitsch, L. (2002). High cycle fatigue resistance and reliability assessment of flexible printed circuitry. *J. Electron. Packag.* 124: 254.

84 Eberl, C., Spolenak, R., Kraft, O., Kubat, F., Ruile, W., and Arzt, E. (2006). Damage analysis in Al thin films fatigued at ultrahigh frequencies. *J. Appl. Phys.* 99: 113501.

85 Sun, X.J., Wang, C.C., Zhang, J., Liu, G., Zhang, G.J., Ding, X.D., Zhang, G.P., and Sun, J. (2008). Thickness dependent fatigue life at microcrack nucleation for metal thin films on flexible substrates. *J. Phys. D-Appl. Phys.* 41: 6.

86 Zhang, G.P., Sun, K.H., Zhang, B., Gong, J., Sun, C., and Wang, Z.G. (2008). Tensile and fatigue strength of ultrathin copper films. *Mater. Sci. Eng. A* 483-484: 387.

87 Eve, S., Huber, N., Last, A., and Kraft, O. (2009). Fatigue behavior of thin Au and Al films on polycarbonate and polymethylmethacrylate for micro-optical components. *Thin Solid Films* 517: 2702.

88 Lewis, J., Greco, S., Chalamala, B., Vick, E., and Temple, D. (2004). Highly flexible transparent electrodes for organic light-emitting diode-based displays. *Appl. Phys. Lett.* 85: 3450.

89 Potoczny, G.A., Bejitual, T.S., Abell, J.S., Sierros, K.A., Cairns, D.R., and Kukureka, S.N., (2013). Flexibility and electrical stability of polyester-based device electrodes under monotonic and cyclic buckling conditions. *Thin Solid Films* 528: 205.

90 Bejitual, T.S., Compton, D., Sierros, K.A., Cairns, D.R., and Kukureka, S.N. (2013). Electromechanical reliability of flexible transparent electrodes during and after exposure to acrylic acid. *Thin Solid Films* 528: 229.

91 Morrow, J. (1968). Fatigue properties of metals. In: *Fatigue Design Handbook, Section 3.2*, Vol. AE-4 (ed. J.A. Graham). Warrendale, PA: Society of Automotive Engineers.

92 Abdallah, A.A., Bouten, P.C.P., Den Toonder, J.M.J., and De With, G. (2008). The effect of moisture on buckle delamination of thin inorganic layers on a polymer substrate. *Thin Solid Films* 516: 1063.

93 Dhakal, T.P., Hamasha, M.M., Nandur, A.S., Vanhart, D., Vasekar, P., Lu, S., Sharma, A., and Westgate, C.R. (2012). Moisture-induced surface corrosion in AZO thin films formed by atomic layer deposition. *IEEE Trans. Dev. Mater. Reliabil.* 12: 347.

94 Pourbaix, M. (1974). *Atlas of Electrochemical Equilibria in Aqueous Solutions*, 2nd English ed. Houston: National Association of Corrosion Engineers.

95 Sierros, K.A., Morris, N.J., Ramji, K., and Cairns, D.R. (2009). Stress–corrosion cracking of indium tin oxide coated polyethylene terephthalate for flexible optoelectronic devices. *Thin Solid Films* 517: 2590.

96 Bejitual, T.S., Morris, N.J., Cronin, S.D., Cairns, D.R., and Sierros, K.A. (2013). Mechano-chemical degradation of flexible electrodes for optoelectronic device applications. *Thin Solid Films* 549: 251.

97 Cardon, A.H., Fukuda, H., Reifsnider, K., and Verchery, G. (eds.) (2000). *Recent Developments in Durability Analysis of Composite Systems*. Rotterdam: A.A. Balkema.

98 Bouchet, J., Pax, G.M., Leterrier, Y., Michaud, V., and Manson, J.A.E. (2006). Formation of aminosilane-oxide interphases. *Compos. Interf.* 13: 573.

99 Singh, B., Bouchet, J., Rochat, G., Leterrier, Y., Manson, J.A.E., and Fayet, P. (2007). Ultra-thin hybrid organic/inorganic gas barrier coatings on polymers. *Surf. Coat. Technol.* 201: 7107.

100 Rogers, J.A., Someya, T., and Huang, Y.G. (2010). Materials and mechanics for stretchable electronics. *Science* 327: 1603.

101 Park, K., Lee, D.K., Kim, B.S., Jeon, H., Lee, J.E., Whang, D., Lee, H.J., Kim, Y.J., and Ahn, J.H. (2010). Stretchable, transparent zinc oxide thin film transistors. *Adv. Funct. Mater.* 20: 3577.

102 Kim, E.-H., Yang, C.-W., and Park, J.-W. (2012). Designing interlayers to improve the mechanical reliability of transparent conductive oxide coatings on flexible substrates. *J. Appl. Phys.* 111.

103 Yang, C.W. and Park, J.W. (2010). The cohesive crack and buckle delamination resistances of indium tin oxide (ITO) films on polymeric substrates with ductile metal interlayers. *Surf. Coat. Technol.* 204: 2761.

104 Miller, D.C., Foster, R.R., Zhang, Y., Jen, S.-H., Bertrand, J.A., Lu, Z., Seghete, D. et al. (2009). The mechanical robustness of atomic-layer- and molecular-layer-deposited coatings on polymer substrates. *J. Appl. Phys.* 105.

105 Leterrier, Y., Medico, L., Demarco, F., Manson, J.A.E., Betz, U., Escola, M.F., Olsson, M.K., and Atamny, F. (2004). Mechanical integrity of transparent conductive oxide films for flexible polymer-based displays. *Thin Solid Films* 460: 156.

106 Zhang, Y.Y. and Gu, Y.T. (2013). Mechanical properties of graphene: Effects of layer number, temperature and isotope. *Comput. Mater. Sci.* 71: 197.

107 De Arco, L.G., Zhang, Y., Schlenker, C.W., Ryu, K., Thompson, M.E., and Zhou, C.W. (2010). Continuous, highly flexible, and transparent graphene films by chemical vapor deposition for organic photovoltaics. *Acs Nano* 4: 2865.

108 Kang, M.G., Park, H.J., Ahn, S.H., and Guo, L.J. (2010). Transparent Cu nanowire mesh electrode on flexible substrates fabricated by transfer printing and its application in organic solar cells. *Solar Energy Mater. Solar Cells* 94: 1179.

109 Li, Y., Mao, L., Gao, Y., Zhang, P., Li, C., Ma, C., Tu, Y., Cui, Z., and Chen, L. (2013). ITO-free photovoltaic cell utilizing a high-resolution silver grid current collecting layer. *Solar Energy Mater. Solar Cells* 113: 85.

110 Amendola, V. and Meneghetti, M. (2009). Self-healing at the nanoscale. *Nanoscale* 1: 74.

111 Mauldin, T.C. and Kessler, M.R. (2010). Self-healing polymers and composites. *Int. Mater. Rev.* 55: 317.

112 Lafont, U., Van Zeijl, H., and Van Der Zwaag, S. (2012). Increasing the reliability of solid state lighting systems via self-healing approaches: A review. *Microelectron. Reliabil.* 52: 71.

113 Lu, C.C., Lin, Y.C., Yeh, C.H., Huang, J.C., and Chiu, P.W. (2012). High mobility flexible graphene field-effect transistors with self-healing gate dielectrics. *Acs Nano* 6: 4469.

114 Baliga, S.R., Ren, M., and Kozicki, M.N. (2011). Self-healing interconnects for flexible electronics applications. *Thin Solid Films* 519: 2339.

115 Odom, S.A., Chayanupatkul, S., Blaiszik, B.J., Zhao, O., Jackson, A.C., Braun, P.V., Sottos, N.R., White, S.R., and Moore, J.S. (2012). A self-healing conductive ink. *Adv. Mater.* 24: 2578.